The Effects of Non-Metallic Inclusions on Charpy V-Notch Toughness

Sunday Abraham[1], Rick Bodnar[1], Eric Lynch[1] and Yufeng Wang[1]

[1]SSAB Americas
1755 Bill Sharp Boulevard
Muscatine, IA 52761 USA
Phone: +1.563.381.5774
Email: Sunday.Abraham@ssab.com; Rick.Bodnar@ssab.com; Eric.Lynch@ssab.com; Yufeng.Wang@ssab.com

ABSTRACT

Non-metallic inclusions are generally considered to be detrimental to the mechanical properties of steel. However, different properties of steel are affected differently by inclusion type, morphology, size, population density and distribution pattern. Since inclusions cannot be entirely eliminated from steel, the residual inclusions need to be engineered to minimize their harmful effects. The accepted and standardized methods of inclusion indexing are largely qualitative and unsuitable for engineering analysis. This paper provides an analysis of the relationships between some of the proposed quantitative methods for inclusion indexing and describes a method for quantifying inclusion-matrix interaction, and its relationship to steel Charpy V-notch toughness.

Keywords: Non-metallic inclusions, Cleanliness, Inter-particle spacing, Inclusion-Matrix Interaction, Charpy Toughness.

INTRODUCTION

Inclusions have varying effects on the performance of steel. While some inclusions are good for steel for certain applications, for example, free-machining steel,[1,2] inclusions are mostly detrimental to other properties of steel.[3-5] The harsher the environment in which steel is applied, the more stringent the requirement for its inclusion content becomes. The requirement for cleanliness is particularly stringent for steel for application in a) tire cord, which due to the small cord diameter of about 0.15 mm is prone to fracture from small inclusions; b) ball- and roller-bearing steels, where service-life depends directly on oxide content which contributes to rolling contact fatigue[6]; c) high strength steel, where high-cycle fatigue properties are important; d) steels for sour service application, where resistance to hydrogen-induced cracking is important; and e) aircraft landing gear where fracture toughness is important. To efficiently engineer inclusions and tailor them to the intended steel application, a deeper knowledge of inclusion evolution during refining in the ladle and casting is required.[7,8]

In addition, to facilitate a proper inclusion engineering strategy, it is important to have an accurate means of determining and characterizing inclusions, use a reliable technique to quantify them, and develop a relationship between the inclusion index and a given property of steel. However, the lack of a clear-cut method for inclusion indexing makes it difficult to establish the effects of certain types of inclusions on product performance or perform a meaningful engineering analysis on the origin of inclusions. The challenge with inclusion indexing is compounded further by the multiple methods used for inclusion analysis in the metallurgical community.[6,9,10] Overall, there are more than two dozen methods available for non-metallic inclusion analysis. Of these methods, the light optical microscope method is widely used by steelmakers due to its simplicity and relatively short turnaround time. However, the cleanliness rating obtained with the optical microscope is highly subjective and unsuitable for engineering analysis. The availability of commercial software, which is capable of summarizing the large volume of data output from the SEM (scanning electron microscope) and EDS (energy dispersive spectroscopy) within a reasonable period of time and in a manner suitable for engineering evaluation, has made the SEM/EDS technique more reliable and attractive. Since the SEM/EDS technique provides detailed information regarding the chemistry, size, morphology and distribution of inclusions, these data can be further used in engineering analysis for process improvement and product development. By combining the information obtained from SEM analysis with the physical and thermal properties of inclusions, one can gain a better understanding of the impact of non-metallic inclusions on a given property of steel. The disparity between the physical (elastic behavior) and thermal properties (coefficients of thermal expansion/contraction) of inclusions and steel can result in perturbation of externally applied stresses and considerable stress accumulation at inclusion-

matrix interface[4,11-13]. At a critical stress level, formation of voids at the inclusion-matrix interface is inevitable. Hard and brittle oxide inclusions that are weakly bonded to the matrix, for example, alumina inclusions, can negatively impact the toughness of steel because voids tend to form at the inclusion-matrix interface and coalesce at the onset of straining. On the other hand, inclusions that are highly deformable and have higher coefficients of thermal expansion or contraction compared to the matrix, for example, manganese sulfides, can cause de-cohesion at the inclusion-matrix interface leading to formation of voids. Such voids typically have sharp edges making it easier for them to propagate and coalesce when the material is strained. This is why manganese sulfides are among the most deleterious inclusions as far as toughness of steel is concerned. The magnitude of the stress field created at the inclusion-matrix interface is dependent on chemistry, size and morphology of the inclusion, as well as the environment in which the material is being used. Therefore, for adequate engineering analysis of the impact of inclusions on a given property of steel, it is important to properly identify and classify all inclusions present in the steel.

This paper compares some of the quantitative techniques for the assessment of non-metallic inclusions, discusses the development of a new quantitative technique based on the nature of inclusion-matrix interaction potential and shows the relationship between inclusion-matrix interaction potential and Charpy V-notch toughness of steel.

A BRIEF REVIEW OF INCLUSION AND CLEANLINESS INDEXING TECHNIQUES

Abraham, et al.[14] provided a comprehensive review of the different techniques proposed for quantification of inclusions. In this paper, only a couple techniques that are relevant to the current work are discussed.

Standard Chart Methods:
The ASTM E45 Methods or their equivalents describe a procedure for assigning inclusions to a category based on similarity in morphology to comparative charts.[15,16] Typically, a 160 mm^2 polished area is observed with a light optical microscope at 100X magnification. Standard reference charts depicting a series of typical inclusion configurations (size, type and number) have been created for direct comparison with the microscopic field of view. In such microscopy methods, inclusions are classified into four types based on their morphology and two subcategories based on their thickness or diameter (Heavy and Thin Series). A - Sulfide Type, B - Alumina Type, C - Silicate Type and D - Globular Oxide Type define their shape while categories Heavy and Thin describe their thickness. Although the types contain chemical names that imply knowledge of their chemical content, the ratings are based strictly on morphology. The chemical names associated with the various types were derived from historical data collected on inclusions found in these shapes and morphologies. The four types are partitioned into Severity Levels based on the number or length of the particles present in a 0.50 mm^2 field of view. There are five methods described in the ASTM E45 standard for cleanliness rating. Method A is based on inclusion worst fields, Method B is based on inclusion minimum length, Method C is used for rating oxides and silicates, Method D is used for rating steel with low inclusion contents, and Method E is used for rating the inclusion content of steels in a manner that reflects the severity and frequency of occurrence of the larger B- and D-type inclusions. The standard chart methods are the conventional technique of rating inclusions and still widely used in the industry today. Although the standard chart methods are useful for a quick assessment of the cleanliness of the steel, they are not suitable for engineering analysis or research purposes.

Oxygen and Sulfur Contents of Steel:
Oxygen and sulfur contents of steel have been used as an indirect measurement of the oxide and sulfide contents of the steel. However, this is not very common anymore, because the performance of the steel is also affected by the types of inclusions.[17,18]

Inclusion Volume Fraction:
Pickering[11] has demonstrated that the ductility of steel has an exponential relationship to the volume fraction of second phase particles, such as manganese sulfides, oxide inclusions or carbides. For particles that are uniformly distributed, the simplest procedure for estimating volume fraction of a particular particle is through calculation of the area fraction, since area fraction is considered to be an estimate of the volume fraction of particles. Hence, correlation of mechanical properties of steel to volume fraction of second phase particles is widely used due to its simplicity. The volume or area fraction of second phase particles can be expressed as:

$$V_V \approx A_A = \frac{\sum A_\alpha}{A_T} \tag{1}$$

where $\sum A_\alpha$ is the sum of the areas of the phase of interest, α, and A_T is the total measurement area.

The use of volume fraction for assessing the cleanliness of steels with respect to the non-metallic inclusions is useful and it will be shown later to have a relationship to the expression for interparticle spacing[14]. It is generally accepted that the interparticle spacing conveys a better physical meaning than the volume fraction, especially for clean steels where the volume fraction of inclusions is small.

The Nearest-Neighbor Distance:

The average center-to-center spacing, $\overline{D}$, between a particle and its nearest neighbor in a random three-dimensional array of particles was formulated by Chandrasekhar.[19-21] When measured between particles intersected by a random straight line through the array, this spacing is given by Equation 2:

$$\overline{D} = \frac{1}{N_L} = \frac{\pi}{6f}\left(1 + \frac{\sigma_{A1}^2}{\overline{x}_{A1}^2}\right)\overline{x}_{A1} \quad (2)$$

where $\overline{D}$ is the average particle spacing, N_L is the number of particles per unit length, f is particle volume fraction, $\overline{x}_{A1}$ is the arithmetic mean of particle diameter, and σ_{A1} is the arithmetic standard deviation.

Inclusion Interparticle Spacing:

Abraham, et al.[14] derived an equation for calculating average spacing between inclusions based on SEM/EDS automated inclusion analysis results. The derived expression describes a relationship between inclusion area and the scanned specimen area during automated inclusion analysis, as shown in Equation 3.

$$\lambda_T = \sqrt{\frac{A_{Scan} - \sum_{i=1}^{n} A_i}{n}} = \sqrt{\frac{A_{Scan}(1 - f_i)}{n}} \quad (3)$$

where λ_T is the Total Interparticle Spacing (TIS) in µm, A_{Scan} is the scanned area during automated SEM analysis, A_i is total area occupied by inclusions, n is the number of inclusions, and f_i is the area fraction of all inclusions in the steel.

Equation 3 can be used to calculate interparticle spacing for different types of inclusions of interest, e.g., MnS interparticle spacing. The relationship between inclusion interpaticle spacing and other methods for quantifying inclusion contents of the steel was studied and then, the inclusion interparticle spacing was correlated to the toughness of the steel as described in the "results and discussion" section of this paper.

EXPERIMENTAL PROCEDURE

For the study, steel samples were secured from 12.5 mm thick plates for room temperature transverse Charpy V-notch (CVN) testing and to generate transverse CVN energy transition curves. 12.5 mm gauge was chosen to ensure that full CVN specimens represent the bulk of the product. The selected chemistries of and processing information for the three products involved in the study are summarized in Table I. The chemistries of the steels within each group are similar and the inclusion-forming elements are within the ranges provided. CVN testing was conducted in accordance to the requirements by ASTM E23. Testing was performed for a temperature range of -90 to 80°C to generate full CVN energy transition curves. Samples for automated SEM/EDS inclusion analysis were secured adjacent to the location of the CVN specimens. Automated SEM/EDS inclusion analyses were performed using a Zeiss Ultra 55 Field Emission Scanning Electron Microscope (FESEM) with AZtec software for inclusion classification. Light microscopy examination of specimens etched in 2% Nital were conducted to measure through-thickness Vickers hardness in the medium-carbon heat treated plates, determine ferrite fractions in the medium-carbon plates and ferrite grain size in medium-carbon and low-carbon plates. Ferrite fractions and grain sizes were determined by automatically scanning an area of 4 mm^2 using a light microscope equipped with the Clemex® image analysis software. Strap transverse tensile specimens with 2" reduced section were machined from the medium-carbon and low-carbon plates for testing.

Table I: Selected Chemistry of Steels, wt %

Product Identification	Processing	C	Mn	S	Ca	Al	N	Si	Other
Medium-Carbon Heat-treated	Austenitized + Quenched	0.190 to 0.210	1.35 to 1.40	0.0001 to 0.0015	0.0008 to 0.0023	0.050 to 0.059	0.0023 to 0.0049	0.230 to 0.260	Nb, Ti, B
Medium-Carbon High Sulfur	Hot Rolled	0.160 to 0.170	1.09 to 1.14	0.0018 to 0.0076	0.0017 to 0.0026	0.023 to 0.028	0.0073 to 0.0108	0.020 to 0.050	V
Low-Carbon High Sulfur	Hot Rolled	0.070 to 0.077	1.22 to 1.30	0.0016 to 0.0050	0.0013 to 0.0025	0.030 to 0.044	0.0081 to 0.0108	0.174 to 0.240	V

RESULTS AND DISCUSSION

Relationship Between Different Methods of Cleanliness Assessment:
The inclusion contents in different steels were quantified using several methods. Inclusion number density, area or volume fraction, mean free path, nearest neighbor distance and interparticle spacing are quantitative and expected to correlate to each other. Examples of the correlation between inclusion interparticle spacing and these quantitative techniques are provided in Figures 1 and 2. The ASTM E45 Method A technique is subjective and hence, it cannot be correlated to quantitative techniques. However, ASTM E2142 Method 1, an SEM/EDS analog of Test Method E45, eliminates the subjectivity associated with using light light microscopy for inclusion characterization. By using ASTM E2142 Method 1 to classify inclusions and employing the indexing technique proposed in ISO 4967 to calculate the arithmetic mean of severity (index) for each type of inclusion, it was found that a decent correlation between inclusion interparticle spacing and the index exists for inclusions of the thin series (Figure 3).

Microstructure and Tensile Testing:
A summary of the microstructure and tensile testing results is provided in Table II. The microstructure in the heat-treated plates comprises of 100% martensite. The through-thickness Vickers hardness values range from 454 to 478. The ferrite fractions in the medium-carbon samples range from 73 to 78% and the grain size ranges from 10 to 14 μm. The ferrite fraction and ferrite grain size in the low-carbon samples range from 85 to 94% and 13 to 17 μm, respectively. In both the medium-carbon and low-carbon samples, no correlation was found between the grain sizes and the CVN impact energies. The difference in Vickers hardness values of the heat-treated product only shows a very weak relationship to the CVN energies. The 0.2% yield and tensile strengths of the medium-carbon and low-carbon plates are within a narrow range. Based on these results, the difference in hardness, strength and ferrite grain size within each groups is considered very small. As a result, differences in CVN toughness between groups can largely be attributed to differences in steel cleanliness.

The CVN energy transition curves were generated using the Origin 9.0 software from OriginLab®. The curves generated were based on Boltzmann's sigmoid function, which describes characteristic "S"-shaped curves. Examples of the generated full energy transition CVN curves are shown in Figure 4. With the equation, the upper shelf energy and transition temperatures (based on the average of the sum of highest and lowest impact energies) were determined. The determined upper shelf energies and ductile-to-brittle transition temperatures were correlated to the non-metallic inclusion contents of the steel.

Correlation of Inclusion Interparticle Spacing to CVN Energy:
Inclusion interparticle spacing has been correlated to CVN impact testing results for heat treated steel, medium-carbon steel with high sulfur level and low-carbon steel with high sulfur level. Figure 5 shows a fair correlation between inclusion oxide interparticle spacing and room temperature CVN energies in the heat-treated steel. Figure 6 equally shows good correlation between inclusion sulfide interparticle spacing and CVN impact energy (upper shelf and room temperature energies in a medium-carbon steel with high sulfur level). In the low-carbon steel with high sulfur level, no correlation was found between the sulfide interparticle spacing and upper shelf or room temperature CVN impact energies. However, it was found that the sulfide interparticle spacing correlates well to the ductile-to-brittle transition temperature (Figure 7). It is possible that with the range of inclusion population densities we are dealing with here, the higher ferrite fraction in the low-carbon steels plays a more significant role on its resistance to fracture at room temperature than inclusions. At lower temperatures, the effect of the higher ferrite fraction diminishes due to the greater stress concentration at the inclusion-matrix interface. Although good relationships were established between inclusion interparticle spacing and CVN impact energy, a deeper understanding of the effect of inclusions on the performance of steel requires consideration of the nature of the interaction of inclusions and matrix[22-26], as discussed in the next section.

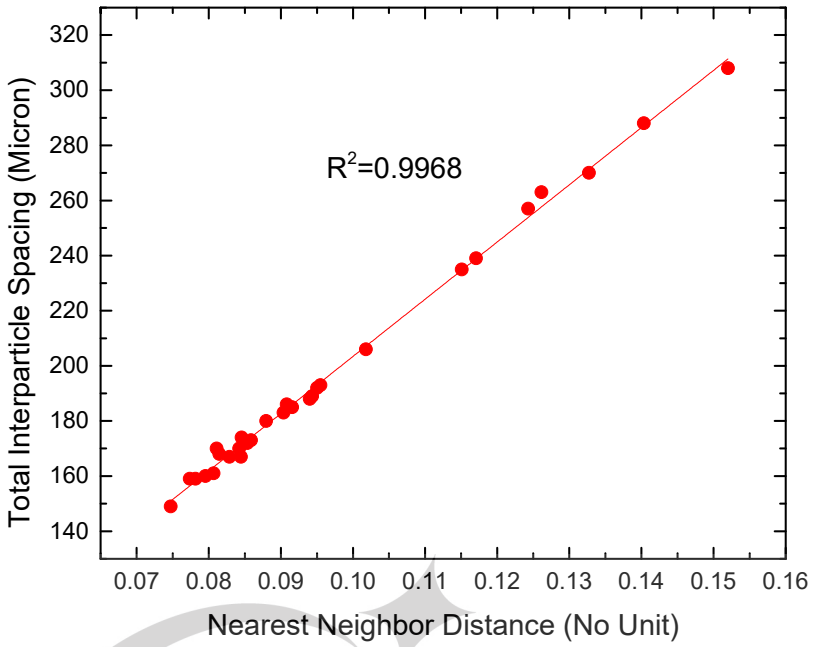

Figure 1: Inclusion Interparticle Spacing vs. Nearest Neighbor Distance

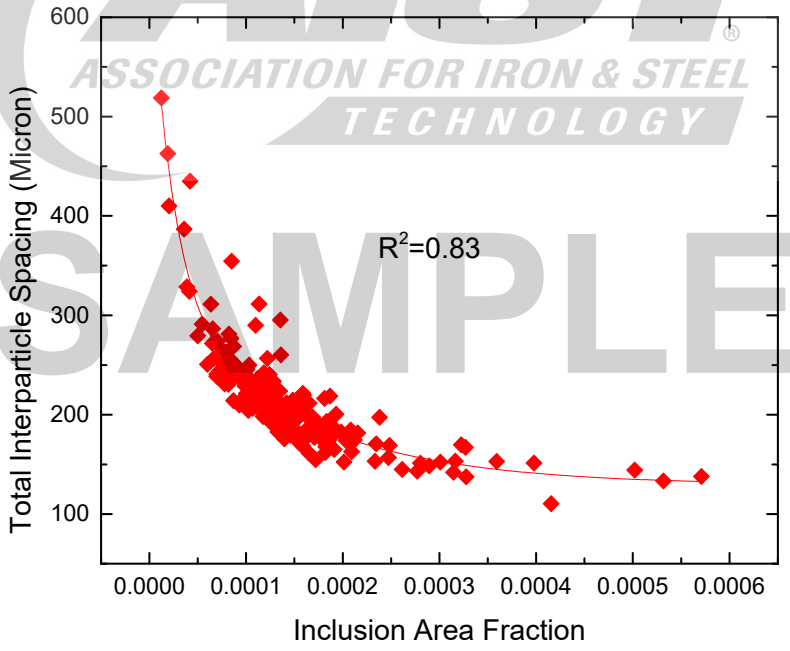

Figure 2: Inclusion Interparticle Spacing vs. Inclusion Area Fraction

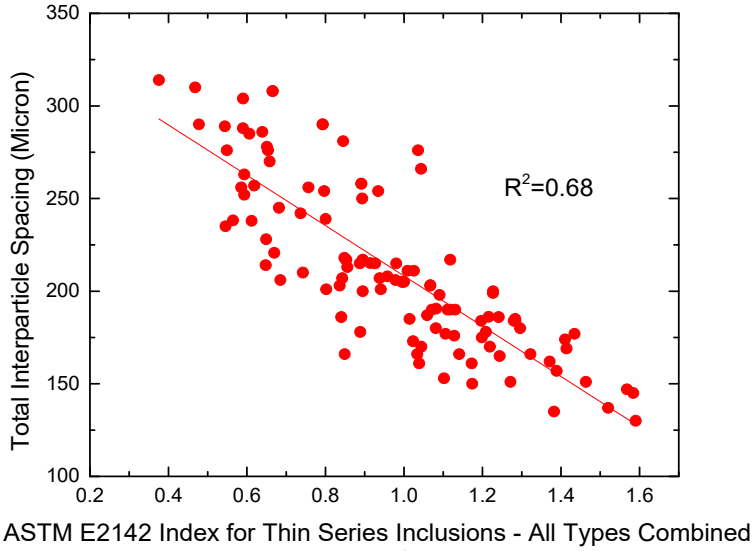

Figure 3: Inclusion Interparticle Spacing vs. ASTM E2142 Inclusion Index

Table II: Microstructure, Hardness and Tensile Testing Results

Sample Type	0.2% Yield Strength (MPa)	UTS (MPa)	HV (1000gf)	Microstructure	Polygonal Ferrite Grain Size (µm)
Medium-Carbon Heat-treated	N/A	N/A	454-478	100% martensite	N/A
Medium-Carbon High Sulfur	390-420	518-562	N/A	73 to78% ferrite + pearlite	10 to 14
Low-Carbon High Sulfur	380-410	472-502	N/A	89 to 94% ferrite + pearlite	13 to 17

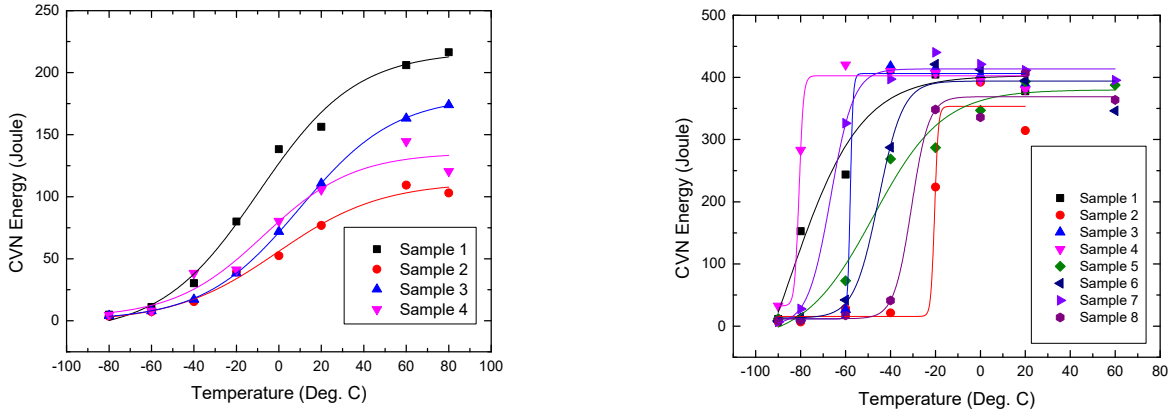

(a) (b)

Figure 4: Example Full Transverse CVN Energy Transition Curves for Medium-Carbon High Sulfur (a) and Low-Carbon High Sulfur (b) Steels

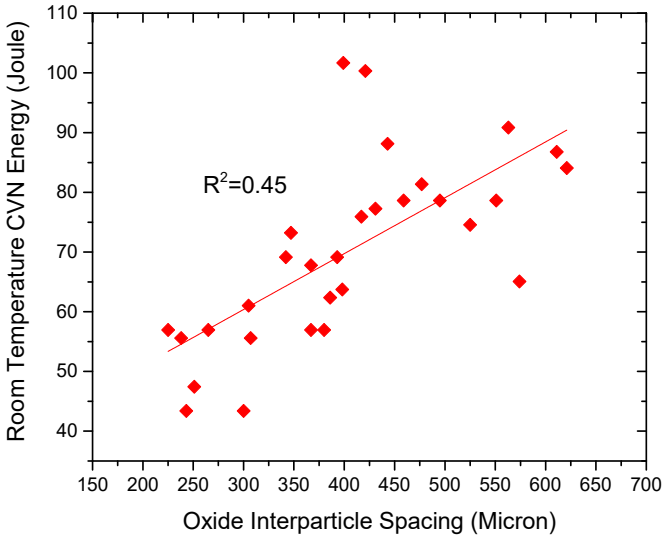

Figure 5: Oxide Interparticle Spacing vs. Room Temperature Transverse CVN Energy for the Heat-Treated Steel

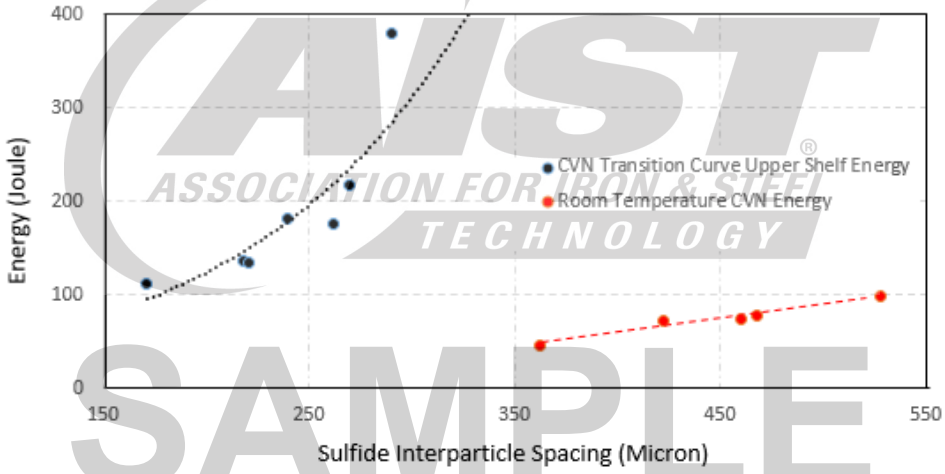

Figure 6: Sulfide Interparticle Spacing vs. CVN Impact Energy (Transverse Specimens)

Correlation of Inclusion-Matrix Strain Energy to CVN Energy:

Laszlo studied stresses generated in materials as a function of the bulk physical properties of the components of the materials.[27-32] He referred to the internal stresses resulting from the difference in the bulk physical properties of the components of a given material as "tessellated stress". Lazlo derived an expression for calculating internal strain energy resulting from tessellated stresses (U), as shown in Equation 4:

$$U = \frac{\varepsilon_i \varepsilon_o X_i (1 - X_i)}{\varepsilon_i X_i + \varepsilon_o (1 - X_i)} \lambda^2 \tag{4}$$

where $\varepsilon_i$is the elastic constant of the particle in the case of inclusions; $\varepsilon_o$is the elastic constant of the material, $X_i$is the volume fraction of the particle; and $\lambda = (\alpha_o - \alpha_i X_i)\Delta T$. $\alpha_o$is the coefficient of thermal expansion of steel; $\alpha_i$is the coefficient of thermal expansion of inclusion and $\Delta T$is the change in temperature. The elastic constant of any material is given by Equation 5.

$$\varepsilon = \frac{mE}{(m-1)} \tag{5}$$

where m is the inverse of Poisson's ratio and E is Young's modulus of elasticity.

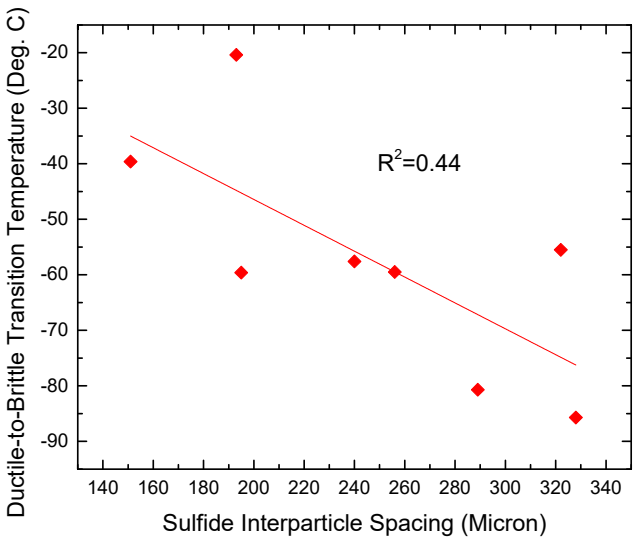

Figure 7: Sulfide Interparticle Spacing vs. Ductile-to-Brittle Transition Temperature (Transverse CVN Specimens) for the Low-Carbon Steel

Equation 4 was used to calculate the strain energy at the inclusion-matrix interface for a given volume fraction and change in temperature for different types of inclusions. The physical properties of different inclusions were taken from different sources.[30-33] The inclusion-matrix interface strain energy is plotted as a function of the difference in coefficients of thermal expansion of the matrix and inclusions, as shown in Figure 8. It can be seen that in the group of stress-raising inclusions, SiO_2 is the most deleterious, and in the group of void-forming inclusions, MnS is the most deleterious. Al_2O_3 inclusions are also more detrimental compared to the $CaO.Al_2O_3$ family of inclusions. Therefore, the total matrix-inclusion interface strain energies due to unmodified alumina and manganese sulfide inclusions were calculated and correlated to CVN upper shelf and room temperature energies for heat treated and high-sulfur medium-carbon steels. The results are summarized in Figures 9 and 10. A good correlation was found between unmodified oxide strain potential and room temperature CVN and upper shelf energies of the steel. A full CVN energy transition curve was also developed for low-carbon steel. Similar to the correlation to sulfide interparticle spacing, it was found that the unmodified sulfide void forming potential does not correlate to the upper shelf energy. However, the unmodified sulfide void-forming potential correlates well to the ductile-to-brittle transition temperature, as shown in Figure 11. The upper shelf energies for the samples of low-carbon steel are relatively the same despite the difference in inclusion population density.

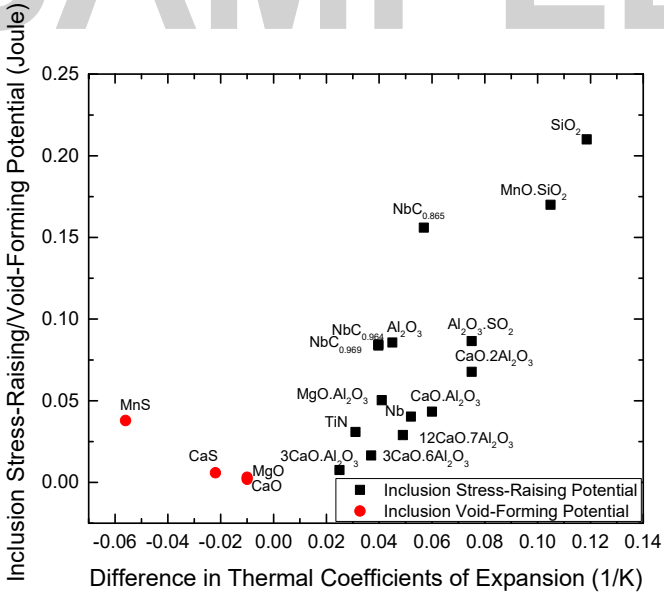

Figure 8: Inclusion-Matrix Strain Energy vs. Difference in Coefficient of Thermal Expansion of Matrix and Inclusion

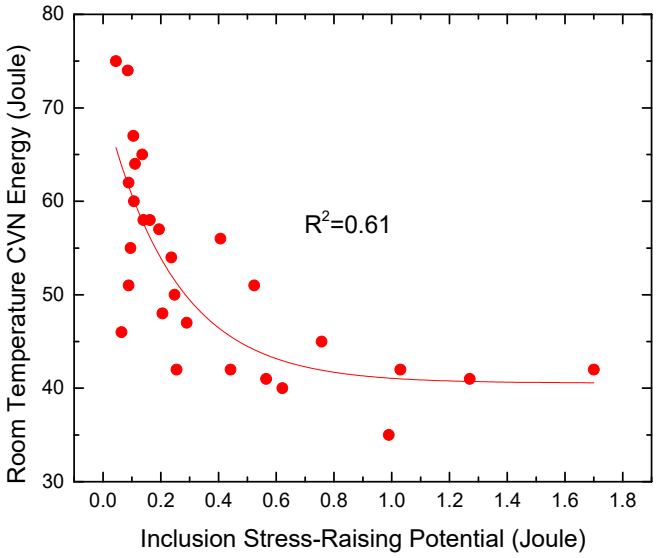

Figure 9: Room Temperature Transverse CVN Energy vs. Unmodified Oxide Stress-Raising Potential for the Heat Treated Steel

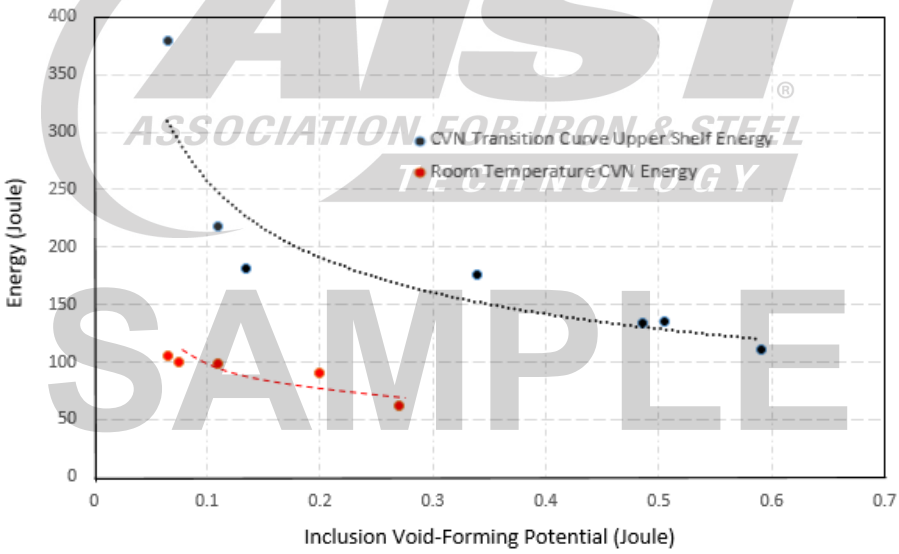

Figure 10: CVN Impact Energy (Transverse CVN Specimens) vs. Unmodified Sulfide Void-Forming Potential for the Medium-Carbon Steel

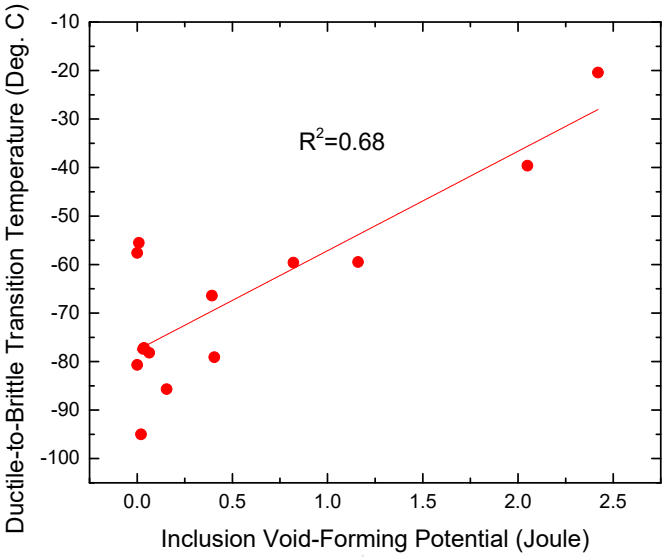

Figure 11: Ductile-to-Brittle Transition Temperature (Transverse CVN Specimens) vs. Unmodified Sulfide Void-Forming Potential for the Low-Carbon Steel

Inclusion-Matrix Strain Energy and Inclusion Engineering:

In aluminum-killed steel, the residual alumina in the steel needs to be modified prior to casting to prevent potential nozzle clogging and minimize the detrimental effect of alumina on the performance of the steel[26]. Calcium is typically employed for the modification process. During calcium treatment, different types of calcium aluminate inclusions are formed. These inclusions have varying degrees of clogging tendency. The lower the melting point, the higher the wettability of the inclusion by the steel and hence, the lower the clogging tendency. The melting points of alumina and calcium aluminate inclusions are plotted with the strain energies of inclusions in Figure 12. Inclusions with low melting points (below steelmaking temperatures) have lower inclusion-matrix interface strain energy compared to alumina inclusions. Figure 13a shows the dependence of oxide (alumina) modification and stress-raising potential on Ca/O ratio for steels containing very low sulfur levels (<0.0010%). Oxide modification is determined based on the fraction of calcium aluminates with melting points below that of steel. It can be concluded from Figure 13a that low oxygen potential is critical for adequate inclusion modification and minimizing stress at the inclusion-matrix interface. Calcium treatment is also performed to prevent the precipitation of MnS during casting. The formation of CaS through calcium treatment is favorable to the properties of steel because of the resulting reduction in void-forming potential. Figure 13b shows the dependence of sulfide modification and void-forming potential on Ca/S ratio for steels with manganese content of about 1.35% and sulfur levels in the range of 0.0015 to 0.0076%. Sulfide modification is determined based on the fraction of sulfides with %Ca>%Mn. It can be seen that at Ca/S of ≥1, adequate sulfide modification can be achieved and unmodified sulfide void-forming potential of sulfides can be greatly reduced. In general, it can be surmised that by calcium treating both alumina and manganese sulfides, the chemistries of the inclusions are modified in such a manner that the disparity in the physical and thermal properties between the inclusions and steels is minimized. This reduces the magnitude of external stress perturbation at the inclusion-matrix interface, thereby improving the performance of the steel.

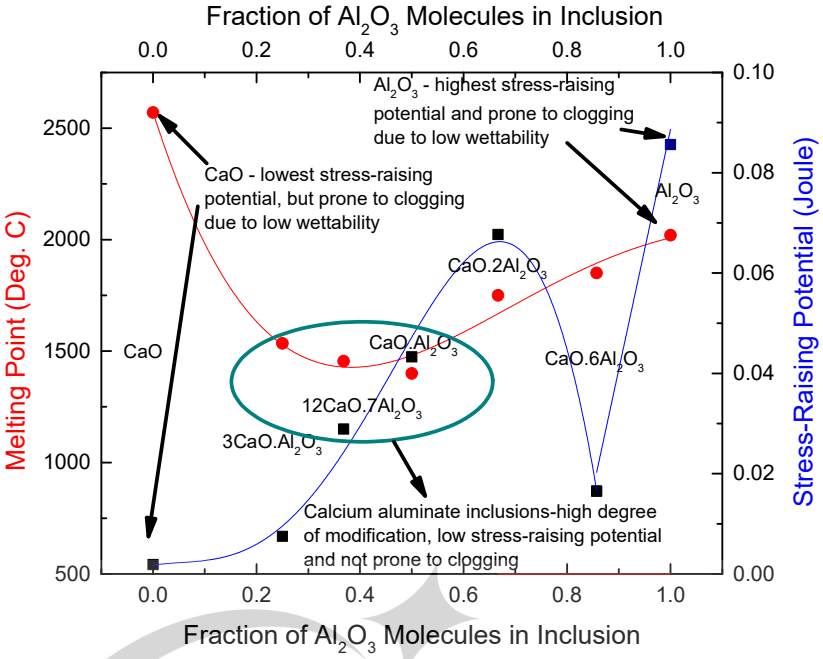

Figure 12: Melting Point of Inclusions and Inclusion-Matrix Interface Energies for Calcium Aluminates

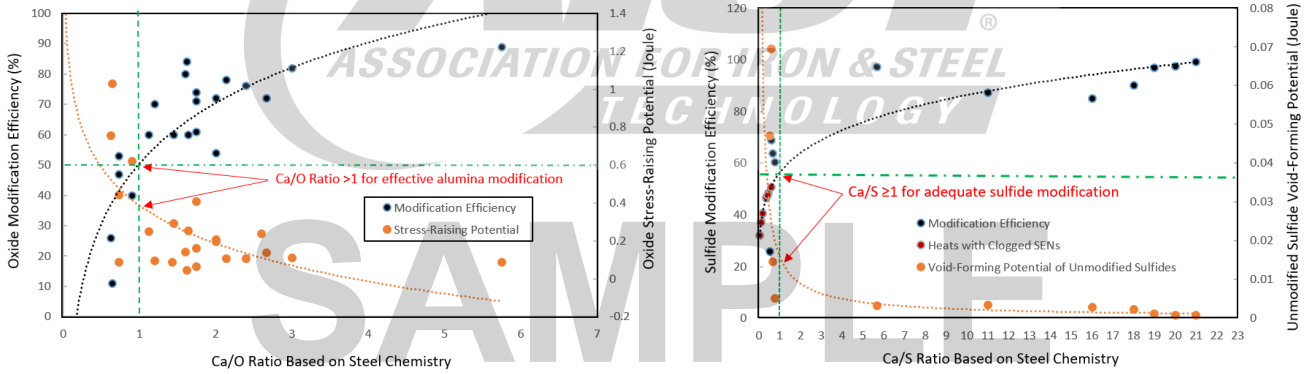

(a) (b)

Figure 13: Relationship between Inclusion Modification and Inclusion-Matrix Interface Stress Field: (a) Ca/O Ratio vs. Oxide Modification Efficiency and Stress-Raising Potential and (b) Ca/S Ratio vs Sulfide Modification and Void-forming Potential

SUMMARY AND CONCLUSIONS

A detailed analysis of the effect of non-metallic inclusions on CVN impact energy has been provided in this paper. It was demonstrated that there is a strong correlation of nearest neighbor distance and inclusion area (volume) fraction to inclusion interparticle spacing. Other quantitative techniques such as mean free path and inclusion number density are expected to have a strong correlation to inclusion interparticle spacing as well. A very good correlation between inclusion interparticle spacing and CVN upper shelf energy in medium-carbon steel was found. In low-carbon steel, however, inclusion interparticle spacing correlates well to CVN energy transition temperature. Inclusion-matrix interface strain energy was calculated for unmodified inclusions. It was shown that the inclusion-matrix interface strain energy also correlates very well to the CVN upper shelf energy in medium-carbon steel and CVN energy transition temperature in low-carbon steel. It appears that both the inclusion interparticle spacing and inclusion-matrix interface strain energy can be used to adequately describe the impact of non-metallic inclusions on the performance of steel.

ACKNOWLEDGMENTS

The authors would like to thank Ben Kowing and SSAB for the permission to publish this paper. Special thanks goes to Brian Castillo for providing the samples used in this study, Matt Werner and Shane Hanssen, who coordinated the testing, Evan Moe, a previous employee of SSAB, and Co-op students (Tristan Pagkalinawan and Hanok Tekle), who performed the CVN impact testing.

REFERENCES

1. N. Anmark, A. Karasev and P.G. Jönsson, "The Effect of Different Non-metallic Inclusions on the Machinability of Steels-Review," *Materials,* Vol. 8, 2015, pp. 751-783.
2. M. Emmendorfer, S.N. Lekakh, L.N. Bartlett, R.J. O'Malley, R. Bodnar, S. Abraham, Y. Wang and M. Werner, "An Investigation of the Machinability of Abrasion Resistant AR450 Steel," *Proc. of MS&T18,* 2018, pp. 479-486.
3. K.O. Findley and E.B. Damm, "The Effects of Non-metallic Inclusions on Mechanical Properties of Steel," *Inclusion Engineering and Clean Steels, Commemorative Volume,* B. Bliss, S. Seetharaman, B. Jones and S. Abraham, eds., Association for Iron & Technology, E-book, 2019, Chapter 5.
4. W.C. Leslie, "Inclusions and Mechanical Properties," *Proc. of Iron and Steel Society of AIME,* 1982, pp. 1-50.
5. R.L. Bodnar and R.F. Cappellini, "Effects of Residual Elements in Heavy Forgings — Past, Present, and Future", *MiCon 86: Optimization of Processing, Properties, and Service Performance Through Microstructural Control,* ASTM STP 979, B.L. Bramfitt, R.C. Benn, C.R. Brinkman, and G.F. VanderVoort, eds., ASTM, Philadelphia, PA, USA, 1988, pp. 47-82.
6. H. Jacobi and K. Wünnenberg, "Methods for Determination of Oxide Cleanness in Steel," *IISI Study on Clean Steel: State of the Art and Process Technology in Clean Steel,* K. Wünnenberg, S. Millman, M. Nadif, C. Marique, M. Sumida and H. Weddige, eds., International Iron and Steel Institute, Belgium, 2004, pp. 287-330.
7. R.J. O'Malley, "Inclusion Evolution and Removal in Ladle Refining," *Inclusion Engineering and Clean Steels, Commemorative Volume,* B. Bliss, S. Seetharaman, B. Jones and S. Abraham, eds., Association for Iron & Steel Technology, E-book, 2019, Chapter 2.
8. L. Zhang, "Inclusion Evolution During Continuous Casting," *Inclusion Engineering and Clean Steels, Commemorative Volume,* B. Bliss, S. Seetharaman, B. Jones and S. Abraham, eds., Association for Iron & Steel Technology, E-book, 2019, 2019, Chapters 3-4.
9. L. Zhang and B.G. Thomas, "State of the Art of in Evaluation and Control of Steel Cleanliness-Review," *ISIJ Int.,* Vol. 43, No. 3, 2003, pp. 271-291.
10. C.R. Cathcart, "Clean Steel Assessment," *Inclusion Engineering and Clean Steels, Commemorative Volume,* B. Bliss, S. Seetharaman, B. Jones and S. Abraham, eds., Association for Iron & Steel Technology, E-book, 2019, Chapter 6.
11. F.B. Pickering, "High-Strength, Low-Alloy Steels – A Decade of Progress," *Micro Alloying 75, Proceedings of an International Symposium on High-Strength, Low-Alloy Steels,* Union Carbide, N.Y., 1975, pp. 9-28.
12. R. Kiessling, *Non-metallic Inclusions in Steel,* The Metals Society, London, 1976, Section Q.
13. K. Yamamoto, H. Yamamura, D. Maeda, and Y. Suwa, "The Effects of Non-metallic Inclusions on Local Ductility," *AISTech 2011 Proceedings,* Vol. II, pp. 507-516.
14. S. Abraham, J. Raines and R. Bodnar, "Development of an Inclusion Characterization Methodology for Improving Steel Product Cleanliness," *Iron & Steel Tech., AIST Trans.,* Vol. 11, No. 2, 2014, pp. 219-234.
15. W.B. Green, "A Brief History, Status, and Mission of ASTM Subcommittee A01.28 on Bearing Steels," *Bearing Steels: Into the 21st Century,* ASTM STP 1327*,* J.J.C. Hoo and W.B. Green, eds., American Society for Testing and Materials, 1998, pp. 3-9.
16. J. Ermigiotti, D. Gallagher, K. Hanratty, E. Moore, E.A. Olcese, K.A. Peters and J.L. Rosiak, "Metals Test Methods and Analytical Procedures," ASTM Standard, Section Three, 2011, pp. 207-1271.
17. R. Kiessling, "Clean Steel – A Debatable Concept," *Swedish Symposium on Non-metallic Inclusions in Steel,* Sweden, 1981, pp. 7-18.
18. M. Hekkanen, "Inclusion Rating for Clean Steels," B.Sc. thesis, Örebro University, Sweden, 2009.
19. S. Chandrasekhar, "Stochastic Problems in Physics and Astronomy," *Rev. Mod. Phys.,* Vol. 15, 1943, pp. 1-89.

20. C.W. Corti, P. Cotterill, and G.A. Fitzpatrick, "The Evaluation of the Interparticle Spacing in Dispersion Alloys," *International Metallurgical Reviews,* Vol. 19, 1977, pp. 77-88.

21. M.F. Ashby and R. Ebeling, "On the Determination of the Number, Size, Spacing, and Volume Fraction of Spherical Second-Phase Particles from Extraction Replicas," *Transactions of the Metallurgical Society of AIME,* Vol. 236, 1967, pp. 1396-1404.

22. A.A. Farmy and A.N. Ragai, "Thermal-Expansion Behavior of Two-Phase Solids," *J. Applied Phys.,* Vol. 41, No. 13, 1970, pp. 5108-5111.

23. G.P. Tandon and G.J. Weng, "Stress Distribution in and Around Spheroidal Inclusions and Voids at Finite Concentration," *J. Applied Mech.,* Vol. 53, 1986, pp. 511-517.

24. T.J. Barker and J.A. Charles, "Influence of Deformed Inclusions on the Short Transverse Ductility of Hot-rolled Steel," *Proceedings, British Steel Corp./Iron and Steel Inst. Conference,* Scarborough, U.K., 1977, pp. 79-87.

25. D.P. Fairchild, D.G. Howden and W.A.T. Clark, "The Mechanism of Brittle Fracture in a Microalloyed Steel: Part II. Mechanistic Modeling," *Metallurgical and Materials Transactions A,* Vol. 31A, 2000, pp. 653-667.

26. S. Abraham, R. Bodnar, J. Raines and Y. Wang, "Inclusion Engineering and Metallurgy of Calcium Treatment," *J. Iron Steel Res. Int.,* Vol. 25, No. 2, February 2018, pp. 133-145.

27. F. Laszlo, "Tessellated Stresses - Part I," *J. Iron Steel Inst.,* Vol. CXLVII, No. 1, 1943, pp.173-199.

28. F. Laszlo, "Tessellated Stresses - Part II," *J. Iron Steel Inst.,* Vol. CXLVIII, No. 2, 1943, pp.137-159.

29. F. Laszlo, "Tessellated Stresses – Part III," *J. Iron Steel Inst.,* Vol. CL, No. 2, 1944, pp.183-209.

30. F. Laszlo. "Tessellated Stresses – Part IV," *J. Iron Steel Inst.,* Vol. CLII, No. 2, 1945, pp.207-229.

31. D. Brooksbank and K.W. Andrews, "Stress Fields Around Inclusions and Their Relation to Mechanical Properties," *J. Iron Steel Inst.,* Vol. 210, No. 4, 1972, pp. 246-255.

32. K.W. Andrews and D. Brooksbank, "Stresses Associated with Inclusions in Steel: A Photoelastic Analogue and The Effects of Inclusions in Proximity," *J. The Iron and Steel Inst.,* Vol. 210, No. 10, 1972, pp. 765-776.

33. M.G.V. Cuppari and S.F. Santos, "Physical Properties of the NbC Carbide," *Metals,* Vol. 6, No. 250, 2016, pp. 1-17.